A&A, 687, A16 (2024)
https://doi.org/10.1051/0004-6361/202346504

Astronomy & Astrophysics

New quasars behind the Magellanic Clouds

II. Spectroscopic confirmation of 136 near-infrared selected candidates⋆

Valentin D. Ivanov[1], Maria-Rosa L. Cioni[2], Michel Dennefeld[3], Richard de Grijs[4,5,6], Jessica E. M. Craig[7], Jacco Th. van Loon[7], Clara M. Pennock[7,8], Chandreyee Maitra[9], and Frank Haberl[9]

[1] European Southern Observatory, Karl-Schwarzschild-Str. 2, 85748 Garching bei München, Germany
e-mail: vivanov@eso.org
[2] Leibniz-Institut für Astrophysik Potsdam, An der Sternwarte 16, 14482 Potsdam, Germany
[3] Institut d'Astrophysique de Paris (IAP), 98bis Bd Arago, 75014, Paris, France
[4] School of Mathematical and Physical Sciences, Macquarie University, Balaclava Road, Sydney, NSW 2109, Australia
[5] Astrophysics and Space Technologies Research Centre, Macquarie University, Balaclava Road, Sydney, NSW 2109, Australia
[6] International Space Science Institute–Beijing, 1 Nanertiao, Zhongguancun, Hai Dian District, Beijing 100190, PR China
[7] Lennard-Jones Laboratories, Keele University, ST5 5BG, UK
[8] Institute for Astronomy, University of Edinburgh, Royal Observatory, Edinburgh, EH9 3HJ, UK
[9] Max-Planck-Institut für extraterrestrische Physik, Giessenbachstrasse 1, 85748 Garching, Germany

Received 26 March 2023 / Accepted 29 March 2024

ABSTRACT

Context. Quasi-stellar objects (QSOs) are a basis for an absolute reference system for astrometric studies. A system like this at the far side of nearby galaxies is required to facilitate measuring of the proper motions of these galaxies. However, the foreground contamination from the galaxies themselves is a problem for the QSO identification.
Aims. We search for new QSOs behind the two Magellanic Clouds, the Magellanic Bridge, and the Magellanic Stream.
Methods. We identify QSO candidates with a combination of near–infrared colors and variability criteria from the public ESO Visual and Infrared Survey Telescope for Astronomy (VISTA) Magellanic Clouds (VMC) survey. We confirm their nature from broad emission lines with low-resolution optical spectroscopy.
Results. We confirmed the QSO nature of 136 objects. They are distributed as follows: 12 behind the Large Magellanic Cloud, 37 behind the Small Magellanic Cloud, 63 behind the Bridge, and 24 behind the Stream. The QSOs span a redshift range from z∼0.1 to z∼2.9. A comparison of our quasar selection with the Quaia quasar catalog, based on *Gaia* low-resolution spectra, yields a selection and confirmation success rate of 6–19%, depending on whether the quality of the photometry, the magnitude ranges, and the colors are considered. Our candidate list is rather incomplete, but the objects in it are likely to be confirmed as quasars with a probability of ∼90%. Finally, we report a list of 3609 objects in the entire VMC survey that match our color and variability selection criteria; only 1249 of them have *Gaia* counterparts.
Conclusions. Our combined infrared color and variability criteria for the QSO selection prove to be efficient: ∼90% of the observed candidates are bona fide QSOs and allow us to generate a list of new high-probability quasar candidates.

Key words. surveys – Magellanic Clouds – quasars: general

1. Introduction

Quasi-stellar objects (QSOs) are distant galaxies with central supermassive black holes that accrete matter from their surroundings. They are only luminous on a scale of a few hundred parsecs, and they therefore appear as point-like objects.

Quasar candidates are often selected based on optical or infrared (IR) variability (Hook et al. 1994; Carnerero et al. 2023; Treiber et al. 2023) radio emission (Gregg et al. 1996; Tuccillo et al. 2015) X-ray (Shanks et al. 1991; Waddell et al. 2024) or mid–IR colors (Lacy et al. 2004; Sajina et al. 2022). Multi-wavelength selections are also used (DiPompeo et al. 2015; Spiniello & Agnello 2019). Bona fide QSOs are confirmed by their broad emission lines (although the absence of these lines does not imply that the object is not a QSO), which also help to derive their redshifts (Vanden Berk et al. 2001). Millions of these objects are known today (Flesch 2023, 2024; Storey-Fisher et al. 2024; Onken et al. 2023) and the lists continue to be updated with the latest surveys.

Quasars provide insights into the structure and evolution of galaxies and are cosmological probes of the intervening interstellar medium. They can also serve as an absolute astrometric reference frame as distant unmoving point-source objects. This reference frame is required to measure the small proper motions (PMs) within nearby galaxies. However, it is challenging to identify QSOs behind these galaxies because of the rich and diverse stellar content of the galaxies themselves, which blurs the boundaries of the stellar locus. Furthermore, the internal reddening inside the foreground galaxies modifies the QSO colors, especially the optical colors.

It is difficult to find QSOs at the far side of the nearby Magellanic Cloud system because of the foreground contamination. It is particularly difficult to find them behind the Small

⋆ Full tables 1, 2, 4 and B.1 are available at the CDS via anonymous ftp to cdsarc.cds.unistra.fr (130.79.128.5) or via https://cdsarc.cds.unistra.fr/viz-bin/cat/J/A+A/687/A16

Magellanic Cloud (SMC) because it exhibits a notable depth and is associated with it stronger source confusion (de Grijs & Bono 2015). Nevertheless, a significant number of QSOs was identified there by studies that specifically targeted this region (Blanco & Heathcote 1986; Dobrzycki et al. 2002, 2003a,b, 2005; Geha et al. 2003; Kozłowski & Kochanek 2009; Kozłowski et al. 2012, 2013, 2011; Véron-Cetty & Véron 2010).

Optical searches can confuse QSOs with stars (van Loon & Sansom 2015; Pennock et al. 2022) or miss more highly obscured QSOs. Searches at radio (Pennock et al. 2021) or near– and mid–IR wavebands can help to alleviate the latter problem. This prompted us to search for QSOs in the VISTA (Visual and Infrared Survey Telescope for Astronomy; Emerson et al. 2006) Survey of the Magellanic Clouds system (VMC; Cioni et al. 2011). The largest single spectroscopically confirmed sample of quasars so far, 758 QSOs, was an OGLE (Optical Gravitational Lensing Experiment Udalski et al. 1992) follow-up by Kozłowski et al. (2013), and more recently, by the Quaia survey based on the low-resolution (R∼30) *Gaia* spectra (Storey-Fisher et al. 2024). Our main goal is to increase the number of known quasars behind the Large and Small Magellanic Clouds, aiming to improve the proper motion reference system. We reported our first results, 37 (34 new) QSOs, also spectroscopically confirmed, in Ivanov et al. (2016). This is the second paper in our series, with further spectroscopy from Very Large Telescope (VLT) and South African Astronomical Observatory (SAAO).

2. Sample selection

2.1. VMC

The VMC is an ESO public survey with a footprint of 184°[2] on the sky around the Large Magellanic Cloud (LMC), the SMC, the Magellanic Bridge, and the Magellanic Stream. The photometry reaches a signal-to-noise ratio S/N∼10 at K_s=20.3 mag (Vega system) in three epochs in the Y and J bands and in 12 epochs in the K_s band. More epochs are available for some tiles[1] and in the areas of overlapping tiles. The time series span nearly eight years. The VMC science is diverse and includes star formation and star formation history, galaxy structure, star clusters, various types of stars (e.g., RR Lyrae and Cepheids), proper motions, background galaxies, and even distant quasars.

The VMC is carried out at VISTA, which is a 4.1m telescope located on Cerro Paranal, equipped with VIRCAM (VISTA InfraRed CAMera; Dalton et al. 2006), which is a near-IR wide-field ∼1×1.5°[2]) camera. The data are reduced with the VISTA Data Flow System (VDFS; Irwin et al. 2004; Emerson et al. 2004) at the Cambridge Astronomical Survey Unit[2]. Their photometric calibration is described in González-Fernández et al. (2018). The data products are available at the ESO Science Archive Facility[3] or at the VISTA Science Archive (VSA; Cross et al. 2012)[4].

2.2. Quasar candidate selection

The criteria for identifying QSO candidates from VMC were defined by Cioni et al. (2013) from 117 known QSOs in a ($Y-J$) versus ($J-K_s$) color–color diagram (Fig. 1) and from their K_s-band variability, requiring that the absolute value of the light-curve slope exceeds a certain limit of |Slope|>10^{-4} mag day^{-1}. The light-curve slope was determined from a simple linear fit of the K_s band versus the time of observations in days, and the adopted limit was based on the behavior of the same known quasars. The quasars were selected with the data available at the time of the Phase 2 submission (DR6 plus some additional images, typically one per tile). Since then, some data have been reprocessed and more observations have become available. An inspection of updated light curves and slope measurements from them (Fig. 2) showed that a significant number of the spectroscopically confirmed quasars fall below the adopted limit, which means that a more stringently defined criterion needs to be adopted in the future, for example, based on a damped random walk (Kelly et al. 2009).

Here, as in Ivanov et al. (2016), we applied the same criteria on 18 mostly peripheral tiles: 3 tiles in the LMC, 7 tiles in the SMC, 6 tiles in the Bridge, and 2 tiles in the Stream. We selected 142 candidates: 15 candidates in the LMC, 40 candidates in the SMC, 63 candidates in the Bridge, and 24 candidates in the Stream. The Bridge and Stream tiles yield more candidates per tile because the foreground contamination from the Magellanic Clouds and the extinction are lower. The observations were carried out under vastly diverse weather conditions because the constraints of the program were relaxed. This allowed a seeing of up to 2″ and thin cloud coverage.

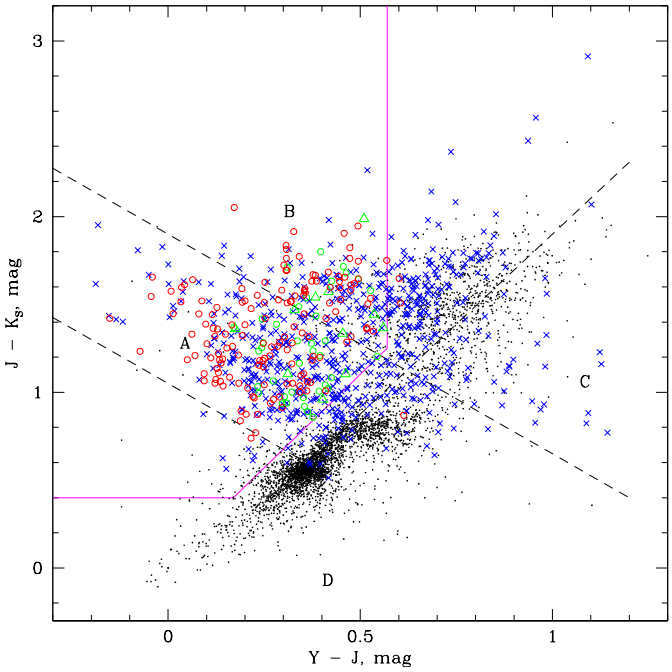

Fig. 1. Color–color diagram showing the color selection of candidates. The dashed lines identify regions (labeled with letters) with known QSOs, and the solid magenta line marks the blue border of the planetary nebulae locus (Cioni et al. 2013). The confirmed QSOs from this work are plotted as red open circles. The open green circles and triangles mark QSOs and non-QSOs from Ivanov et al. (2016), respectively. The blue crosses indicate VMC counterparts to the spectroscopically confirmed QSOs from Kozłowski et al. (2013, VMC photometry selected within a matching radius of 1″). The black dots are randomly drawn LMC objects (with errors in all three bands <0.1 mag) to mark the main stellar locus; some of those in regions B and C are contaminating background galaxies.

[1] Tiles are contiguous images that combine six pawprints taken in an offset pattern; a pawprint is an image obtained on an individual VIRCAM pointing that generates an image with gaps between the detectors. See Cioni et al. (2011) for a description of the VMC observing strategy.
[2] http://casu.ast.cam.ac.uk/
[3] http://archive.eso.org/cms.html
[4] http://vsa.roe.ac.uk/

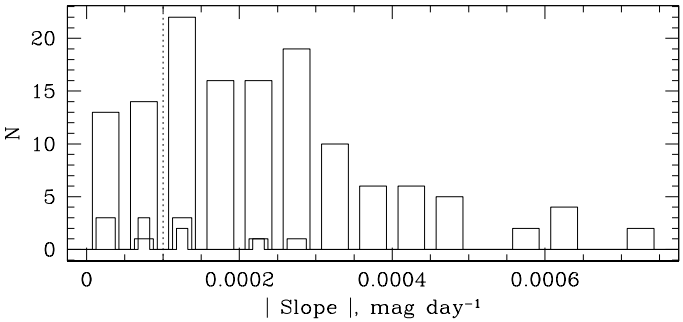

Fig. 2. Histogram of the absolute slopes from the linear fit to the light curves of the objects in this paper: classified as QSOs (wide bins), remaining unknown because of poor-quality spectra or lack of prominent emission lines (medium-width bins) and confirmed stars (narrow bins). The vertical dotted line is the QSO selection limit defined by Cioni et al. (2013).

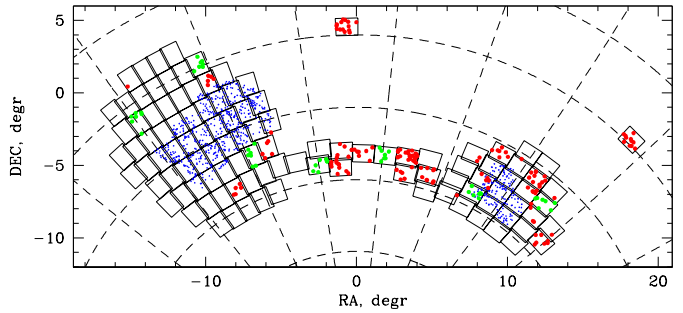

Fig. 3. Location of the objects with spectroscopic follow-up in this work (red) and confirmed QSOs from Kozłowski et al. (2013, blue) and Ivanov et al. (2016, green). The VMC tiles are shown as rectangles. The grid shows lines of constant right ascension and declination (spaced by 15°and 5°, respectively). The coordinates are offset with respect to (α_0, δ_0) = (51°, −69°).

During the selection, we excluded any previously known QSOs and gave preference to the brightest candidates in each tile to optimize the spectroscopic follow-up. Therefore, our results cannot be used to draw strict statistical conclusions. Our main goal is to confirm as many QSOs as possible for future astrometric studies.

Our main target selection was aimed at a VLT follow-up, but spectroscopic confirmation with smaller facilities is also possible. To facilitate this, we performed an identical candidate selection in the entire VMC survey footprint with an additional brightness criterion of Y<18.0 mag to enable a follow-up with a 2 m class telescope. This yielded 36 objects, 15 of which lie in the range Y=16.5–17.4 mag. Seven of these were observed, bringing the total number of objects with follow-up to 151.

Table 1 lists the observed candidates: the VMC identification (Col. 1), coordinates (Cols. 2–3), magnitudes in the YJK_s bands and their photometric errors (Cols. 4–9), and the object identification (Col. 10) used in the spectroscopic observations. The last consists of the VMC tile name and a sequential number in the catalog of sources in that tile; the letter g indicates that a source was extended according to the VDFS pipeline. Ivanov et al. (2016) demonstrated that some low- redshift QSOs fall into this category. The location of the newly confirmed QSOs in the ($Y-J$) versus ($J-K_s$) color-color diagram is shown in Fig. 1. Their positions on the sky are plotted in Fig. 3, and their Y-band finding charts are shown in Fig. A.1.

Appendix B presents the complete list of all VMC survey quasar candidates in the latest internal release (August 2022) that match our color and variability criteria for the benefit of further studies. The color criterion alone yields 163226 objects, and 3609 of these have statistically significant slopes (Slope/$\sigma_{\rm Slope}\geq$3) that exceed the |Slope|=10^{-4} mag day^{-1} limit.

3. Spectroscopic follow-up observations

We selected 142 candidates that were among the brightest in each tile for the follow-up. Their locations were scattered throughout the survey footprint for a better chance of observing them in service mode. Two additional objects (BRI 3_4 046_2 and SMC 6_3 141_2) serendipitously fell into the slits, which increased the total number of observed targets to 144. The selection and observations followed the same procedure as in Ivanov et al. (2016). We used FOcal Reducer and low dispersion Spectrograph 2 (FORS2; Appenzeller et al. 1998) at the VLT (Very Large Telescope) between October 2016 and August 2017 in long-slit mode with the 300V+10 grism, GG435+81 order-sorting filter, and a 1.3″ wide slit. The spectra cover λ=445–865 nm with a resolving power R=$\lambda/\Delta\lambda$~440. Two exposures with integration times between 60 sec and 530 s were taken, depending on the apparent QSO brightness at the time of the VMC observations, which is not necessarily the same as at the moment of the follow-up because the intrinsic QSO variability may render the quasars fainter or brighter. In some cases, we had more exposures because the conditions were too poor for even our relaxed weather constraints or because the observations were interrupted because the telescopes were closed and a full set of observations was obtained on another night. We also exploited the low-quality data as long as emission lines were identifiable. The signal-to-noise ratio typically was ~10–20 at the centre of the wavelength range, at continuum level, and higher at the emission lines. The reduction was performed with the FORS2 pipeline (v. 5.3.23). The spectrophotometric calibration was carried out with standards (Oke 1990; Hamuy et al. 1992, 1994; Moehler et al. 2014a,b), observed and processed as the science spectra. The VLT observing log is given in Table 2.

An additional seven objects (bringing the total number of spectra to 151) were observed with the SpUpNIC[5] (Spectrograph Upgrade: Newly Improved Cassegrain; Crause et al. 2016, 2019) long-slit spectrograph at the 1.9 m telescope at SAAO in November 2017. Grating 7 with no order-separation filter (to extend the spectral coverage; emission lines from the second-order spectra were ignored) was used with a 1.95″ wide slit, delivering a resolving power of R~700–1700 over $\lambda\lambda$=3750–9300 Å. The slit was always oriented East–west, and a single 1800 s exposure was taken for each object. The data reduction was performed in the standard way, with bias and dome flat-field corrections. The wavelength calibration was made with spectra from an internal CuAr lamp, obtained after each science observation to cancel out possible instrument flexures. Feige 110 and LTT 3218 standards (from the same lists as for the VLT) were used to derive the spectral response. The 1.9 m telescope observing log is given in Table 3.

The reduced 148 spectra (for three objects, no 1D spectra could be extracted, usually due to poor weather conditions) are shown in Fig. 4. The emission lines were identified by comparing our spectra with a composite QSO spectrum (Vanden Berk et al. 2001). We typically had several lines; when only one was available, it had to be MgII 2798 Å, because if the line belonged

[5] https://www.saao.ac.za/astronomers/spupnic/

Table 1. VMC coordinates and photometry of QSO candidates (in order of increasing right ascension).

VMC ID	α (J2000) (h:m:s)	δ (d:m:s)	Y (mag)	σ_Y (mag)	J (mag)	σ_J (mag)	K_S (mag)	σ_{K_S} (mag)	Class	object ID
VMC J000041.81−730258.8	00:00:41.81	−73:02:58.8	16.868	0.007	16.334	0.006	14.986	0.006	1	VMC Bright 03 (SMC 4_1)
VMC J000442.82−742013.9	00:04:42.82	−74:20:13.9	18.888	0.020	18.652	0.021	17.498	0.022	−1	SMC 3_1 107
VMC J000505.24−741051.5	00:05:05.24	−74:10:51.5	17.548	0.009	17.053	0.009	15.307	0.007	1	SMC 3_1 044g
VMC J000611.48−645423.7	00:06:11.48	−64:54:23.7	18.211	0.014	17.753	0.013	15.848	0.009	1	STR 2_1 203
VMC J000737.85−733445.6	00:07:37.85	−73:34:45.6	17.878	0.011	17.729	0.013	16.398	0.012	−1	SMC 3_1 119

Notes. The class indicates if the VDFS identified a point-like (−1) or extended (1) morphology. For objects in the bright sample for the SAAO 1.9 m telescope, we list (in the last column, in brackets) the tiles in which they fall; more than one tile is listed for objects in overlapping regions. Only the first five objects are shown for guidance. The entire table is available at the CDS.

Table 2. Log of the VLT spectroscopic observations.

Object ID	UT at start of obs. yyyy-mm-ddThh:mm:ss	Exp. (s)	sec z (dex)	Slit PA (deg)
BRI 2_3 007	2016-12-08T05:42:13.371	60	1.912−1.916	−65.199
BRI 2_3 007	2016-12-08T05:43:58.280	60	1.920−1.923	−65.199
BRI 2_3 011	2016-12-05T00:26:16.593	180	1.562−1.558	30.072
BRI 2_3 011	2016-12-05T00:30:04.451	180	1.559−1.556	30.072
BRI 2_3 032	2016-12-07T06:00:32.486	510	1.913−1.945	−67.766
BRI 2_3 032	2016-12-07T06:10:01.053	510	1.950−1.984	−67.766

Notes. Starting times, exposure times, starting and ending airmass, and slit position angles for each exposure are listed in separate successive lines. Multiple exposures of each object are entered separately. Only the observations of the first three objects are shown for guidance. The entire table is available at the CDS.

Table 3. Log of the 1.9 m SAAO spectroscopic observations.

Object ID	UT at start of obs. yyyy-mm-ddThh:mm:ss	sec z (dex)
VMC SAAO 01 I02	2017-11-23T00:15:11	1.17
VMC SAAO 02 I03	2017-11-27T19:41:13	1.35
VMC SAAO 04 I05	2017-11-22T23:23:11	1.21
VMC SAAO 11 I08	2017-11-23T20:01:21	1.31
VMC SAAO 08 I11	2017-11-24T19:55:06	1.27
VMC SAAO 10 I14	2017-11-28T22:38:57	1.28
VMC SAAO 15 I24	2017-11-28T21:54:58	1.42

Notes. Starting times and the airmass at the start of each exposure are listed. A single 1800 sec exposure was obtained for each object.

Table 4. Derived parameters for the objects in this paper.

Object ID	Spectral feature, observed Central wavelength (Å)	S/N	Redshift z	Class.
BRI 2_4 054	OI/SiII 1305: 5072.93 ± 2.27	14	2.881 ± 0.004	QSO
	CIV 1549: 6012.24 ± 1.35	3		
	CIII] 1909: 7400.55 ± 1.90	3		
BRI 3_4 131	OI/SiII 1305: 5008.19 ± 0.42	5	2.838 ± 0.001	QSO
	CIV 1549: 5946.14 ± 0.45	14	(2.82 ± 0.10)	
	CIII] 1909: 7326.39 ± 1.84	10		
BRI 3_6 090	CIV 1549: 5807.74 ± 2.46	4	2.748 ± 0.002	QSO
	CIII] 1909: 7151.63 ± 1.51	15		
	...			
LMC 8_3 023	None			star
LMC 8_3 095g	None			blue star
SMC 4_2 103	Too low S/N			unkn.
SMC 4_5 062	Too low S/N			unkn.
SMC 5_3 003g	Too low S/N			unkn.
SMC 5_3 021	Balmer lines, CaT			star
SMC 6_3 186g	Too low S/N			unkn.
SMC 6_3 195	Too low S/N			unkn.
SMC 6_3 322	Too low S/N			unkn.
VMC Bright 02	No em. lines, poss. ell. gal.		∼0	unkn.
VMC Bright 03	Too low S/N			unkn.

Notes. Columns contain: detected spectral features and their central wavelengths, S/Ns within ±20 Å from the line centers measured with DER_SNR (Stoehr et al. 2008), estimated redshifts (the colon marks redshifts that we consider tentative due to a single-line identification and low S/N; a second redshift from Quaia is listed for 74 objects in common) and object classifications. Only the beginning and the end of the table is shown for guidance. The entire dataset is available at the CDS.

to a different element or if the redshift was different, other emission lines with comparable strength would have been inside the observed wavelength range (because the S/N was sufficient to detect the MgII), and lines like that were missing. The redshifts were measured as in Ivanov et al. (2016), by fitting emission lines with Gaussian profiles using the IRAF[6] task *splot*. The results are listed in Table 4. Some features at the edges of the spectra or features that were strongly contaminated by sky emission lines or affected by intervening absorption were omitted from the analysis. The statistical errors and errors from wavelength calibration were negligible (see Sect. 3 in Ivanov et al. 2016). We measured the redshift error from different lines of the same object. The finding charts of the objects that were followed up are shown in Fig. A.1.

A single line was observed in some spectra. For example, this occurred for quasars at redshifts between ∼1 and ∼1.4 when the only prominent line within our wavelength range was MgII 2798 Å. The featureless continuum outside of the line excludes the presence of any other lines: When the observed line was CIII] 1909, for instance, then CIV 1549 should have appeared in the blue part of the spectrum. In most cases, the S/N of the spectra was sufficient (we adopted a limit of 10) at the continuum level to exclude the presence of other lines, but this was not always the case. Therefore, some of our redshifts are tentative, and they are marked in Table 4 with colon signs. The table also contains the S/N calculated in the vicinity of each emission line that we used

[6] The Image Reduction and Analysis Facility is distributed by the National Optical Astronomy Observatory, which is operated by the Association of Universities for Research in Astronomy (AURA) under a cooperative agreement with the National Science Foundation.

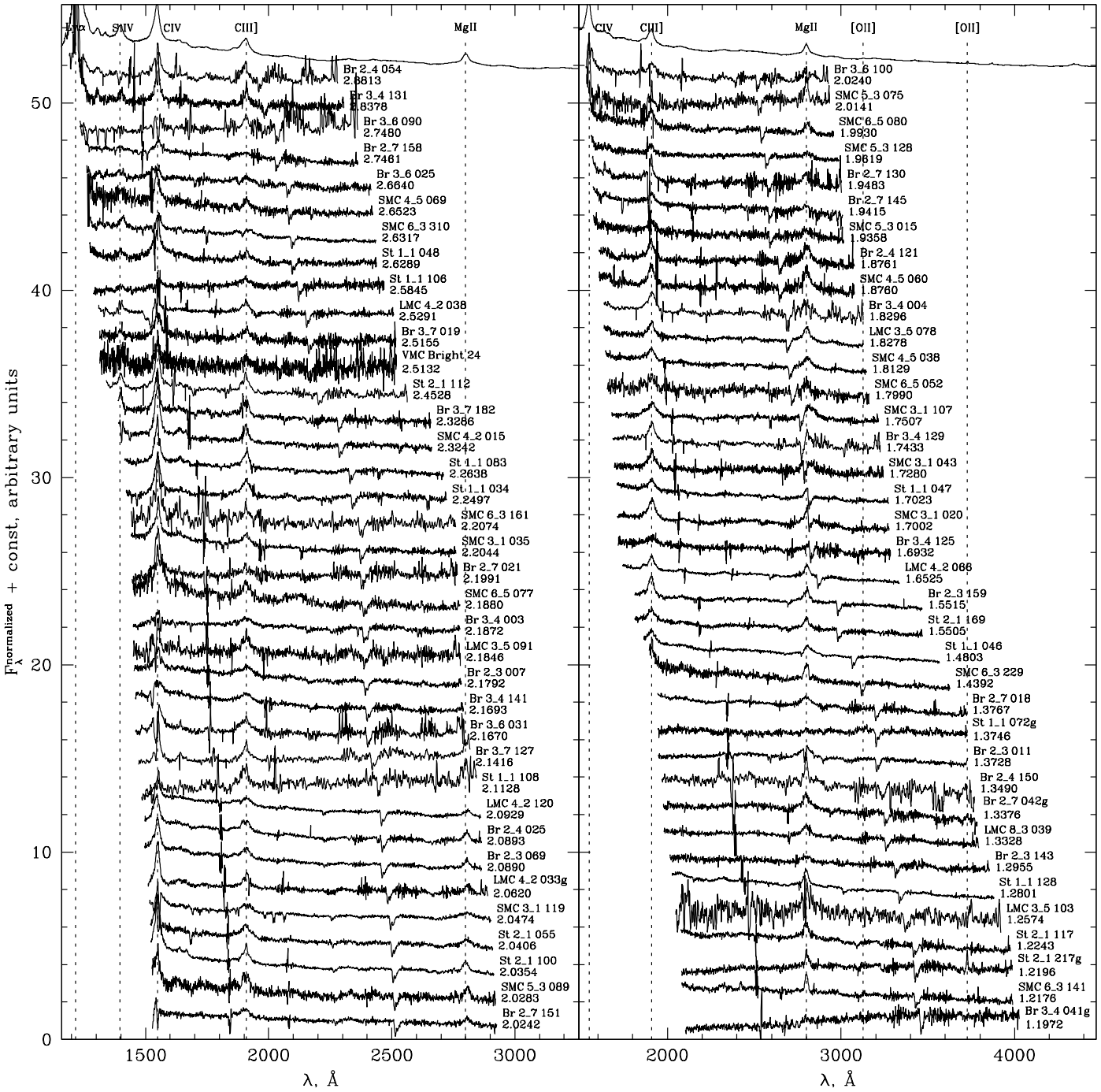

Fig. 4. Spectra of 148 objects (for 3 objects, no spectra could be extracted, usually due to poor weather conditions) sorted by redshift and shifted to the rest-frame wavelength. The spectra were normalized to an average value of one and shifted vertically by offsets of two, four, etc., for display purposes. The SDSS composite QSO spectrum (Vanden Berk et al. 2001) is shown at the top of all panels. Objects without a measured redshift due to a lack of lines or low S/N are plotted assuming z=0 in the fifth panel next to the sky spectrum to facilitate identifying the residuals from the sky emission lines.

to evaluate the redshift. The S/N refers to resolution elements, and therefore, the real S/N for the broad lines is much higher, and the derived errors for the central wavelength especially for the redshift estimates are more relevant. For narrow-line objects, the estimated S/N is dominated by the continuum level and is a lower limit for the line core (e.g., in LMC 3_5 085g, Bridge 3_4 209g, and Bridge 2_7 053g). Finally, for the single-line objects we tentatively assigned redshift errors of 0.005 for $z \leq 1$ and 0.015 for $z > 1$. These are typical values at these redshifts.

4. Results and discussion

4.1. Quasar confirmation

The majority of the candidates, 136 out of 148 observed objects, are bona fide QSOs at z~0.1–2.9 (Fig. 4). They all show some broad emission lines even though some spectra need block averaging, typically by four resolution bins, to make their features clearly evident in the plot (the line measurements were made on the original, not on the smoothed spectra). Lyα is visible in the

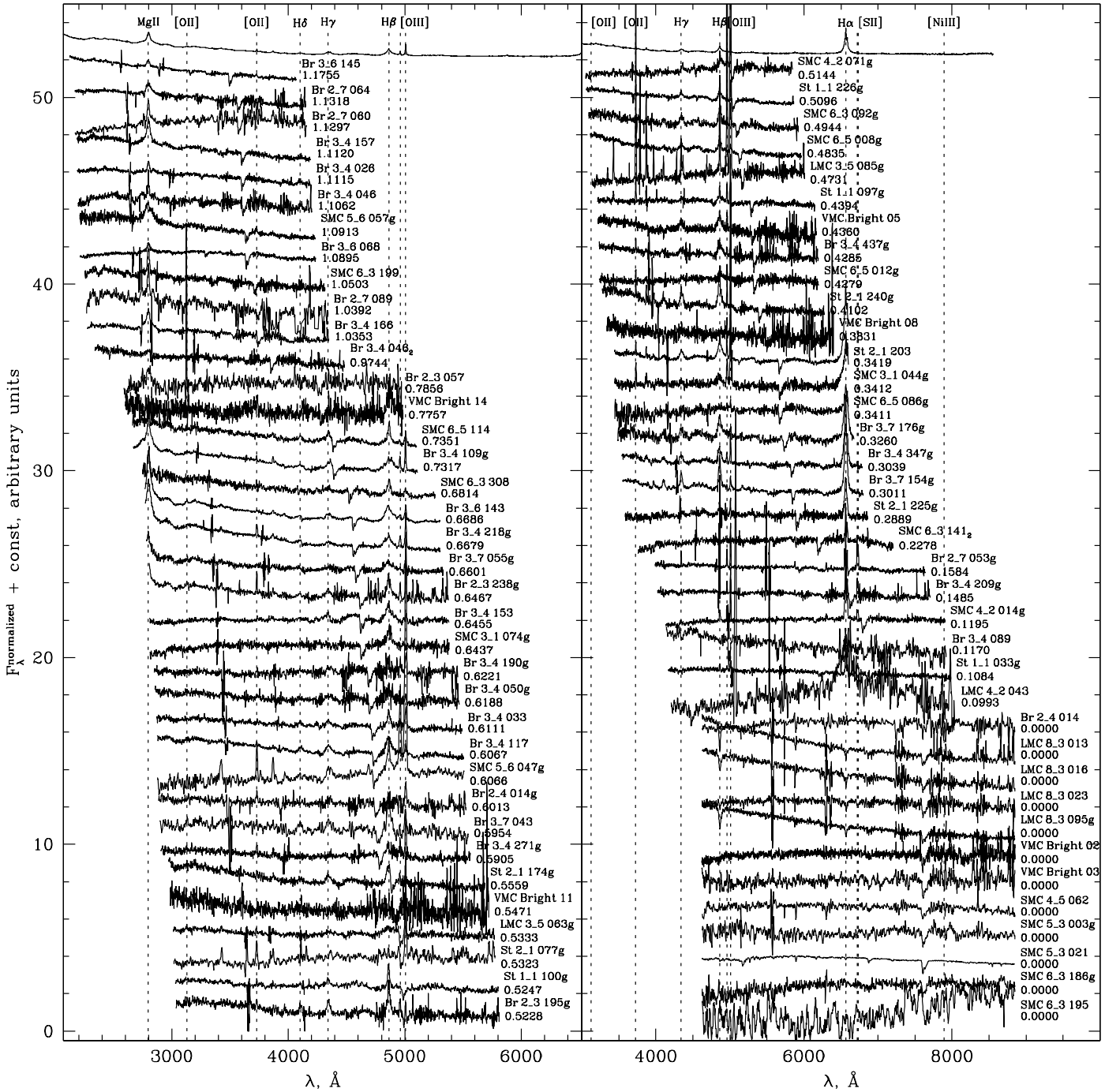

Fig. 4. continued.

spectra of the highest-redshift QSOs, and the remaining sample shows other typical emission lines. The newly confirmed QSOs from the VLT-observed sample are distributed as follows: 11 in the LMC, 34 in the SMC, 62 in the Bridge, and 24 in the Stream areas. The 5 QSOs from the bright candidate list are one in the LMC, 3 in the SMC, and another one in the Bridge. The spectra of six objects appear to be star-like without broad emissions, and nine further objects are too noisy for a secure classification.

The VDFS pipeline classifies 55 of our 151 objects as extended sources, and 49 of these are spectroscopically confirmed QSOs. However, their extended nature seems to be more a matter of foreground contamination from Magellanic Cloud sources than a real resolving of the host galaxy because ten extended QSOs have redshift z>1 and their hosts are unlikely to be resolved under atmospheric seeing conditions. Furthermore, one of the extended non-QSOs is a blue LMC star, and its extended nature is likely due to a surrounding star cluster. Therefore, the VDFS classification cannot be a critical constraint when a QSO candidate sample is assembled.

Figure 5 shows that the fraction of confirmed QSOs with $z\leq1$ is higher here than in Ivanov et al. (2016). The reason likely is that we selected brighter candidates and based our study on a large number of Bridge tiles, in which the reddening of background objects is lower and the foreground contamination is weaker than behind the LMC and SMC. The colors of lower-redshift QSOs are closer to the stellar locus than those of the

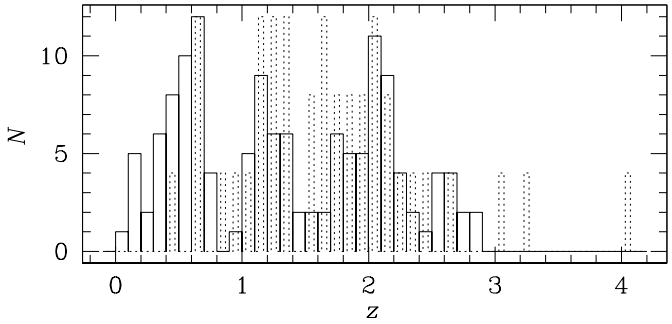

Fig. 5. Redshift histogram for 136 confirmed QSOs (solid line). For comparison, we plot the 47 objects with measured redshift from Ivanov et al. (2016, dashed line).

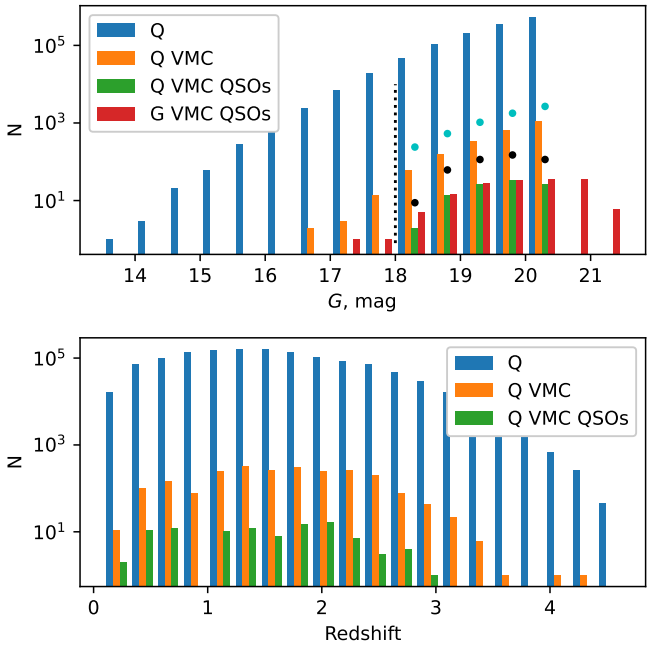

Fig. 6. Parameters of the quasar sample. Top: luminosity functions of quasars from Quaia and the VMC survey in G band. All Quaia quasars (1.3 million objects; blue), Quaia quasars with VMC counterparts with quasar-like colors (2347 objects; orange); spectroscopically confirmed VMC quasars from this paper and from Ivanov et al. (2016) with *Gaia* counterparts (161 objects; red); the same as the red sample, but without the 5 objects from the bright SAAO sample and those that fall below the Quaia G=20.5 mag limit (green), projected output for a VMC survey full quasar sample (450 objects; black dots), and confirmed Quaia quasars scaled down from the full sky to the VMC survey area (~6300 objects; cyan dots), assuming a loss of 10% in the zone of avoidance. In reality, 7386 Quaia quasars fall in the VMC survey footprint. bottom: redshift distribution for all Quaia quasars (1.3 million objects; blue), for Quaia quasars with VMC counterparts with quasar-like colors (2347 objects; orange), and Quaia quasars with spectroscopically confirmed quasars from our VMC selection (161 objects; green). See Sect. 4 for details.

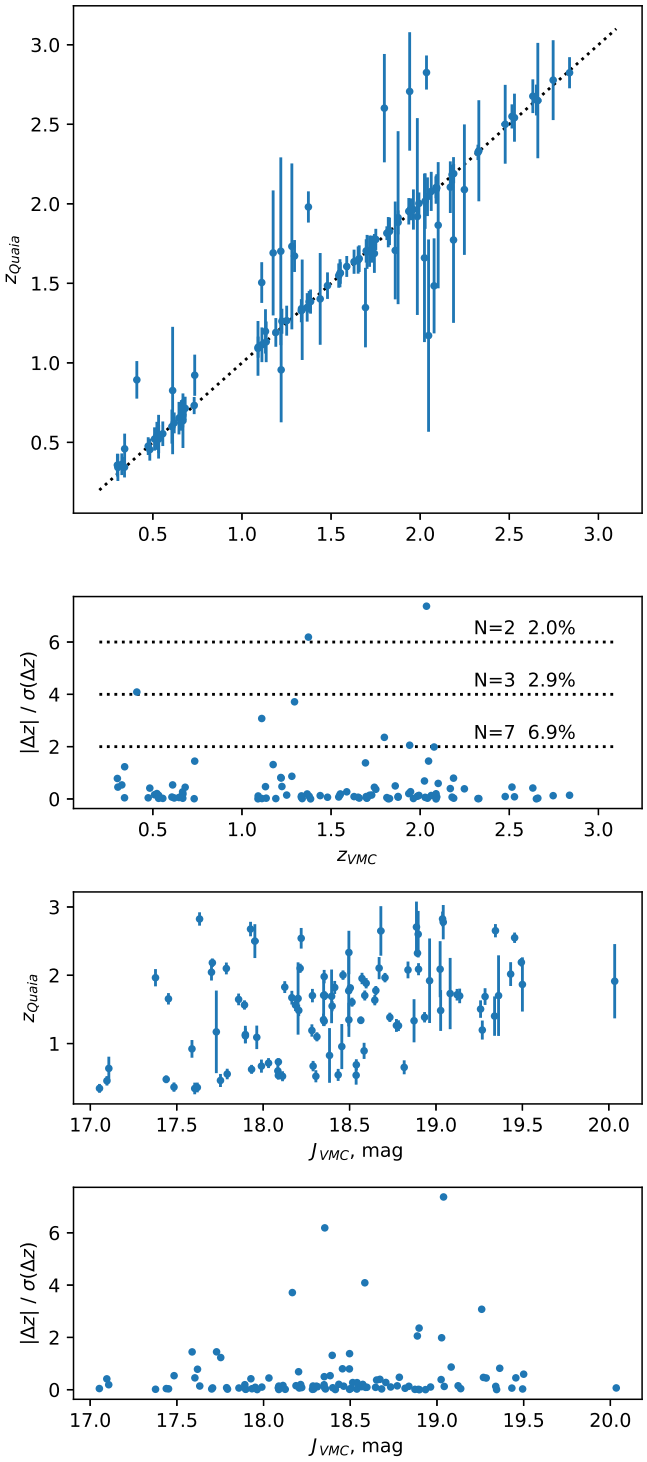

Fig. 7. Comparison of the redshifts from Quaia and from our VLT spectra (top) and absolute values of the differences as function of redshift in units of sigma (bottom). The labels above each dashed line indicate the numbers of quasars above these lines and the corresponding fractions in percentages. See Sect. 4 for details.

higher-redshift QSOs, which makes it harder to identify them in the inner regions of the Magellanic Clouds and easier in the Bridge.

Detections for some of our targets, which are all confirmed quasars, have been reported in the literature: Bridge 3_4 109g and Stream 2_1 174g in UV with GALEX (Galaxy Evolution Explorer; Morrissey et al. 2007); SMC 4_5 060 and SMC 6_3 310 in X-ray with *XMM-Newton* (X-ray Multi-Mirror Mission; Sturm et al. 2013); SMC 6_3 310 and SMC 4_2 071g are listed as new X-ray identified active galactic nucleus candidates by Maitra et al. (2019), also based on *XMM-Newton*, and SMC 4_2 071g and again SMC 4_5 060 were detected in X-ray as well, but with *Chandra* (McGowan et al. 2008). Kim et al. (2012) identified LMC 8_3 039 as a QSO candidate from a combination of light

curves and multicolor criteria, and our spectrum confirms it. To summarize, only a handful of our confirmed QSOs have been detected in X-ray so far because of the sparse coverage with sensitive observations. eROSITA, the soft X-ray instrument on board the Spectrum-Roentgen-Gamma (*SRG*) mission (Predehl et al. 2021), completely covered the region of the Magellanic Clouds during its all-sky surveys. A preliminary investigation of the eROSITA catalog derived from the first all-sky survey data (Merloni et al. 2024) reveals a detection rate up to 30%, depending on matching criteria. More detailed work on the X-ray properties of QSOs behind the Magellanic system is in progress.

4.2. Completeness

Controlling the completeness is not a main goal of this paper. We aim to increase the number of confirmed quasars with the shortest possible observing time, but to still estimate, we turned to the sample of nearly 1.3 million quasars (with G<20.5 mag; Fig. 6, top panel, blue), with secure redshifts from the low-resolution *Gaia* spectra from Storey-Fisher et al. (2024; Quaia). This catalog has its own incompleteness and contamination issues, but the spectroscopic nature of the confirmation, the large number of quasars, and the full coverage of the VMC survey footprint makes it most suitable for this purpose.

First, we determined the number of quasars that our search should find that will also be accessible to Quaia. To compare the output of our spectroscopic confirmation campaign from this work and from Ivanov et al. (2016) with the Quaia sample, we scaled our 102 VLT-confirmed quasars up with Quaia counterparts, with the inverse fraction of the observed tiles. Between this work and Ivanov et al. (2016), we have followed-up 25 out of 110 VMC survey tiles (the seven bright additional objects followed-up at the SAAO are scattered across the entire VMC survey footprint and were ignored here). Extrapolating over the entire VMC survey, we scaled these 102 VLT-confirmed quasars up with G in the overlapping range 18–20.5 mag (to be discussed further) by an area ratio factor of 4.4, arriving at ∼450 VMC survey quasars that we may be able to confirm with the same selection and following the same observing strategy (black dots in Fig. 6, top). This number must be compared with the expected number of Quaia quasars within the VMC survey footprint over an identical magnitude interval.

On one hand, our estimates are optimistic because the tiles in this study are located in the outermost regions in the system, where crowding and confusion are not as problematic as in the innermost regions. On the other hand, it is known that not all quasars are variable and would meet the variability criterion of Cioni et al. (2013). Furthermore, the observations were taken under highly variable weather conditions because our program was designed as a poor-weather filler, and we only followed-up the brightest candidates to optimize telescope time.

To obtain G-band magnitudes for our candidates and confirmed quasars, we cross-identified them with the *Gaia* DR3 main catalog (Gaia Collaboration 2022) within a radius of 0.35″. The results for the former are reported in Table B.1, and for the latter, we show them in the red histogram in the top panel of Fig. 6 for 161 objects (quasars confirmed at the 1.9 m SAAO were excluded for statistical reasons). It appears that 42 (∼24%) of them cannot ever have Quaia counterparts because they fall below its G=20.5 mag limit, and the bright Quaia quasars fall in the VMC saturation regime. Here and throughout, the matching radius was set to make any spurious contamination unlikely: we repeated the cross-identification with modified coordinates, increasing the Dec by 10′ and found only five matches, three of which are with separations >0.9″ and the other two are at 0.25–0.35″. This keeps the spurious contamination at a level of ∼0.1%.

Our quasars are relatively faint because of the saturation of brighter sources in the VMC. Bright quasars are important for studies of intervening absorption lines, for instance, but they only constitute a small fraction: By integrating the Quaia luminosity function above G=16.5 mag, we find that quasars without a single VMC survey counterpart constitute ∼0.1% of the entire Quaia sample, and those that are brighter than G=18.0 mag, which is the brightest limit of our confirmed quasars (dashed black line in the upper panel), constitute only ∼2.3%.

Next, we determined the number of Quaia quasars that are accessible to the VMC survey-based quasar search and follow-up. We cross-identified Quaia quasars with the VMC source catalog (as of DR6): 7386 Quaia quasars fall within the VMC survey footprint; 6923 have matches within 0.35″ radii, but only for 3149 do we have sufficiently good photometry in all three bands without contamination or error flags and errors <0.15 mag; 2347 matches remain when our color-selection criteria are applied. We considered all objects, regardless of their apparent G-band magnitude. However, for a proper comparison, we should exclude objects that are too bright and would saturate in the VMC. They would reside in the brightest bins with $G \lesssim$17.5–18 mag, as shown in Fig. 6. Integration of the Quaia luminosity function above this limit indicates that only ∼2% of Quaia quasars are lost. We therefore ignored them for the purpose of this comparison.

Finally, our expected yield of 450 confirmed quasars within the Quaia apparent magnitude range from the entire VMC survey constitutes ∼6% of all Quaia quasars. This fraction increases to ∼19% of nearly 2350 Quaia quasars that match our color criteria. We speculate that these low fractions are caused by the weak variability of most quasars, which our survey data cannot recognize. This is consistent with our preliminary investigation of the light curves of Quaia quasars with multi-epoch counterparts in the VMC survey: The preliminary investigation suggested that the vast majority of Quaia quasars are indeed not variable enough to meet our minimum light-curve slope criterion. This warrants further investigation and will be reported in another paper.

This result suggests that the complete list of our candidates presented in Table B.1 probably only contains a small fraction of all quasars within the VMC footprint. However, the success rate of our new spectroscopic follow up is ∼90% (∼91% for VLT and ∼71% for 1.9 m), implying that nearly nine of every ten candidates in the list are likely to be confirmed as quasars when a similar spectroscopic follow-up is carried out.

The distribution of redshifts for the entire Quaia (blue), the Quaia quasars with VMC counterparts (orange), and our spectroscopically confirmed quasars with Quaia counterparts (green) are shown in the lower panel of Fig. 6. Our sample is dominated by quasars with a lower redshift than Quaia, probably because we tended to select the brightest candidates in each tile for the follow-up to minimize the observing time per object. Storey-Fisher et al. (2024) verified the quality of their redshifts. A comparison with the redshift derived from our 102 VLT spectra suggests that the main disagreements occur in only a few percent of the cases (Fig. 7). This lends additional credibility to the Quaia catalog. The redshifts that differ are not concentrated toward the faintest objects, but occur over a range of apparent magnitudes, and their Quaia redshift errors are typically significantly larger than for other objects with similar magnitudes.

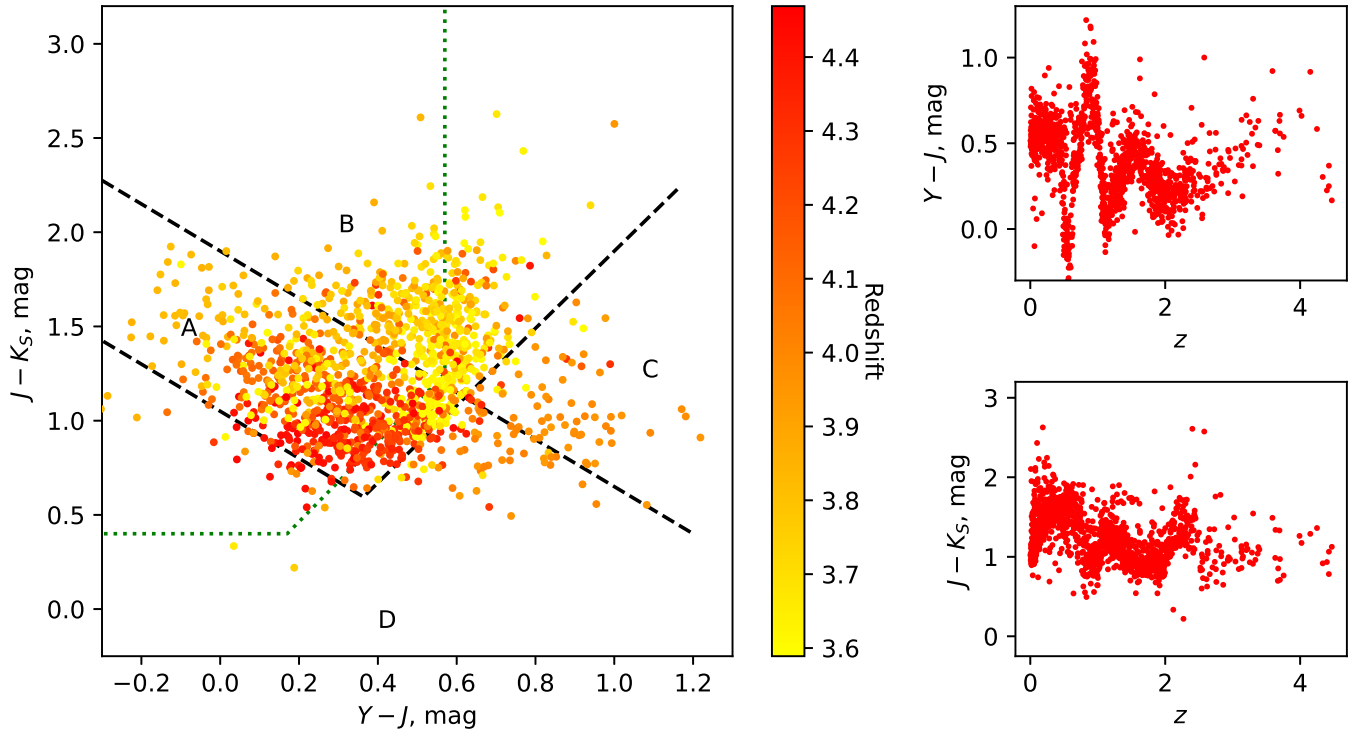

Fig. 8. Left: color-color diagram of all spectroscopically confirmed QSOs with VISTA/VIRCAM photometry. For the notation of the regions, see Fig. 1. Right: $Y-J$ and $J-K_S$ colors as a function of redshift for all spectroscopically confirmed QSOs with VISTA/VIRCAM photometry. The variations are driven by strong emission lines that enter and exit the band passes of individual filters.

4.3. Color-redshift relations

We explored whether the diagnostic color–color diagram that we used to select candidates can help us to constrain their redshift. To expand the statistics, we added to the VMC QSOs the QSOs from the latest catalog of Véron-Cetty & Véron (2010, 13 edition), which were observed with some other VISTA/VIRCAM surveys: VHS (McMahon et al. 2013, 5719 objects), VIDEO (Jarvis et al. 2013, 339 objects), and VVV (Minniti et al. 2010, 5 objects). The color–color diagram coded by redshift is shown in the left panel of Fig. 8. The lowest-redshift QSOs are clustered in a locus at $Y-J$~0.45–0.65 mag and $J-K_S$~1.1–1.8 mag, but the more distant are scattered over the entire diagram. The reason for this behavior is shown in the panels on the right, which show that the two colors vary with redshift. Sharp color changes are visible as various more prominent emission lines enter or exit the bandpasses of individual filters. Therefore, this diagram has the potential of separating only the nearest QSOs.

5. Summary

We spectroscopically confirmed 136 QSOs within the footprint of the Magellanic system. They were selected from their near-IR colors and variability from the ESO VMC public survey. The uniform VMC observations, spanning nearly 8 yr, proved a reliable resource for QSO selection because nearly 90% of the observed candidates were quasars. However, a comparison with the Quaia catalog indicated that our selection recovered only 6–19% of the quasars identified from the *Gaia* low-resolution spectra. The fraction depends on the magnitude range, the quality of VMC survey photometry, and the candidate colors. The fraction appears to be relatively low because most quasars are not sufficiently variable to meet our variability criterion. Our quasar candidate list therefore is far from complete, but the candidates in it are quasars with a high degree of certainty. The variability is an important quasar identification tool, especially for radio-quiet quasars. Finally, we reported a list of 3609 candidates that met our criteria from the entire VMC survey footprint. Based on the previous statistics, we expect that nearly 90% of them will be confirmed as quasars if they are subjected to a spectroscopic follow-up similar to the one described here.

Acknowledgements. This paper is based on observations made with ESO telescopes at the La Silla Paranal Observatory under program IDs 092.B-0104(A), 098.B-0229(A) and 099.B-0204(A). We have made extensive use of the SIMBAD Database at CDS (Centre de Données astronomiques) Strasbourg, the NASA/IPAC Extragalactic Database (NED) which is operated by the Jet Propulsion Laboratory, CalTech, under contract with NASA, and of the VizieR catalog access tool, CDS, Strasbourg, France. We thank Lisa Crause for efficient support at the SAAO telescope. JEMC acknowledges STFC studentship. We thank the anonymous referee for the comments that helped to improve the paper.

References

Appenzeller, I., Fricke, K., Fürtig, W., et al. 1998, The Messenger, 94, 1
Blanco, V. M., & Heathcote, S. 1986, PASP, 98, 635
Carnerero, M. I., Raiteri, C. M., Rimoldini, L., et al. 2023, A&A, 674, A24
Cioni, M.-R. L., Clementini, G., Girardi, L., et al. 2011, A&A, 527, A116
Cioni, M.-R. L., Kamath, D., Rubele, S., et al. 2013, A&A, 549, A29
Crause, L. A., Carter, D., Daniels, A., et al. 2016, SPIE Conf. Ser., 9908, 990827
Crause, L. A., Gilbank, D., Gend, C. v., et al. 2019, J. Astron. Telescopes Instrum. Syst., 5, 024007
Cross, N. J. G., Collins, R. S., Mann, R. G., et al. 2012, A&A, 548, A119
Dalton, G. B., Caldwell, M., Ward, A. K., et al. 2006, SPIE Conf. Ser, 6269, 30
de Grijs, R., & Bono, G. 2015, AJ, 149, 179
DiPompeo, M. A., Bovy, J., Myers, A. D., & Lang, D. 2015, MNRAS, 452, 3124
Dobrzycki, A., Groot, P. J., Macri, L. M., & Stanek, K. Z. 2002, ApJ, 569, L15
Dobrzycki, A., Macri, L. M., Stanek, K. Z., & Groot, P. J. 2003a, AJ, 125, 1330
Dobrzycki, A., Stanek, K. Z., Macri, L. M., & Groot, P. J. 2003b, AJ, 126, 734

Dobrzycki, A., Eyer, L., Stanek, K. Z., & Macri, L. M. 2005, A&A, 442, 495
Emerson, J. P., Irwin, M. J., Lewis, J., et al. 2004, SPIE Conf. Ser., 5493, 401
Emerson, J., McPherson, A., & Sutherland, W. 2006, The Messenger, 126, 41
Flesch, E. W. 2023, Open J. Astrophys., 6, 49
Flesch, E. W. 2024, Open J. Astrophys., 7, 6
Gaia Collaboration 2022, VizieR Online Data Catalog: I/355
Geha, M., Alcock, C., Allsman, R. A., et al. 2003, AJ, 125, 1
González-Fernández, C., Hodgkin, S. T., Irwin, M. J., et al. 2018, MNRAS, 474, 5459
Gregg, M. D., Becker, R. H., White, R. L., et al. 1996, AJ, 112, 407
Hamuy, M., Walker, A. R., Suntzeff, N. B., et al. 1992, PASP, 104, 533
Hamuy, M., Suntzeff, N. B., Heathcote, S. R., et al. 1994, PASP, 106, 566
Hook, I. M., McMahon, R. G., Boyle, B. J., & Irwin, M. J. 1994, MNRAS, 268, 305
Irwin, M. J., Lewis, J., Hodgkin, S., et al. 2004, SPIE Conf. Ser., 5493, 411
Ivanov, V. D., Cioni, M.-R. L., Bekki, K., et al. 2016, A&A, 588, A93
Jarvis, M. J., Bonfield, D. G., Bruce, V. A., et al. 2013, MNRAS, 428, 1281
Kelly, B. C., Bechtold, J., & Siemiginowska, A. 2009, ApJ, 698, 895
Kim, D.-W., Protopapas, P., Trichas, M., et al. 2012, ApJ, 747, 107
Kozłowski, S., & Kochanek, C. S. 2009, ApJ, 701, 508
Kozłowski, S., Kochanek, C. S., & Udalski, A. 2011, ApJS, 194, 22
Kozłowski, S., Kochanek, C. S., Jacyszyn, A. M., et al. 2012, ApJ, 746, 27
Kozłowski, S., Onken, C. A., Kochanek, C. S., et al. 2013, ApJ, 775, 92
Lacy, M., Storrie-Lombardi, L. J., Sajina, A., et al. 2004, ApJS, 154, 166
Maitra, C., Haberl, F., Ivanov, V. D., Cioni, M.-R. L., & van Loon, J. T. 2019, A&A, 622, A29
McGowan, K. E., Coe, M. J., Schurch, M. P. E., et al. 2008, MNRAS, 383, 330
McMahon, R. G., Banerji, M., Gonzalez, E., et al. 2013, The Messenger, 154, 35
Merloni, A., Lamer, G., Liu, T., et al. 2024, A&A, 682, A34
Minniti, D., Lucas, P. W., Emerson, J. P., et al. 2010, New A, 15, 433
Moehler, S., Modigliani, A., Freudling, W., et al. 2014a, The Messenger, 158, 16
Moehler, S., Modigliani, A., Freudling, W., et al. 2014b, A&A, 568, A9
Morrissey, P., Conrow, T., Barlow, T. A., et al. 2007, ApJS, 173, 682
Oke, J. B. 1990, AJ, 99, 1621
Onken, C. A., Wolf, C., Hon, W. J., et al. 2023, PASA, 40, e010
Pennock, C. M., van Loon, J. T., Filipović, M. D., et al. 2021, MNRAS, 506, 3540
Pennock, C. M., van Loon, J. T., Anih, J. O., et al. 2022, MNRAS, 515, 6046
Predehl, P., Andritschke, R., Arefiev, V., et al. 2021, A&A, 647, A1
Sajina, A., Lacy, M., & Pope, A. 2022, Universe, 8, 356
Shanks, T., Georgantopoulos, I., Stewart, G. C., et al. 1991, Nature, 353, 315
Spiniello, C., & Agnello, A. 2019, A&A, 630, A146
Stoehr, F., White, R., Smith, M., et al. 2008, in ASP Conf. Ser., 394, Astronomical Data Analysis Software and Systems XVII, eds. R. W. Argyle, P. S. Bunclark, & J. R. Lewis, 505
Storey-Fisher, K., Hogg, D. W., Rix, H.-W., et al. 2024, ApJ, 964, 69
Sturm, R., Haberl, F., Pietsch, W., et al. 2013, A&A, 558, A3
Treiber, H. P., Hinkle, J. T., Fausnaugh, M. M., et al. 2023, MNRAS, 525, 5795
Tuccillo, D., González-Serrano, J. I., & Benn, C. R. 2015, MNRAS, 449, 2818
Udalski, A., Szymanski, M., Kaluzny, J., Kubiak, M., & Mateo, M. 1992, Acta Astron., 42, 253
van Loon, J. T., & Sansom, A. E. 2015, MNRAS, 453, 2341
Vanden Berk, D. E., Richards, G. T., Bauer, A., et al. 2001, AJ, 122, 549
Véron-Cetty, M.-P., & Véron, P. 2010, A&A, 518, A10
Waddell, S. G. H., Nandra, K., Buchner, J., et al. 2024, A&A, in press, https://doi.org/10.1051/0004-6361/202245572

Appendix A: Finder charts

VMC survey finder charts of the objects we considered are shown in Fig. A.1.

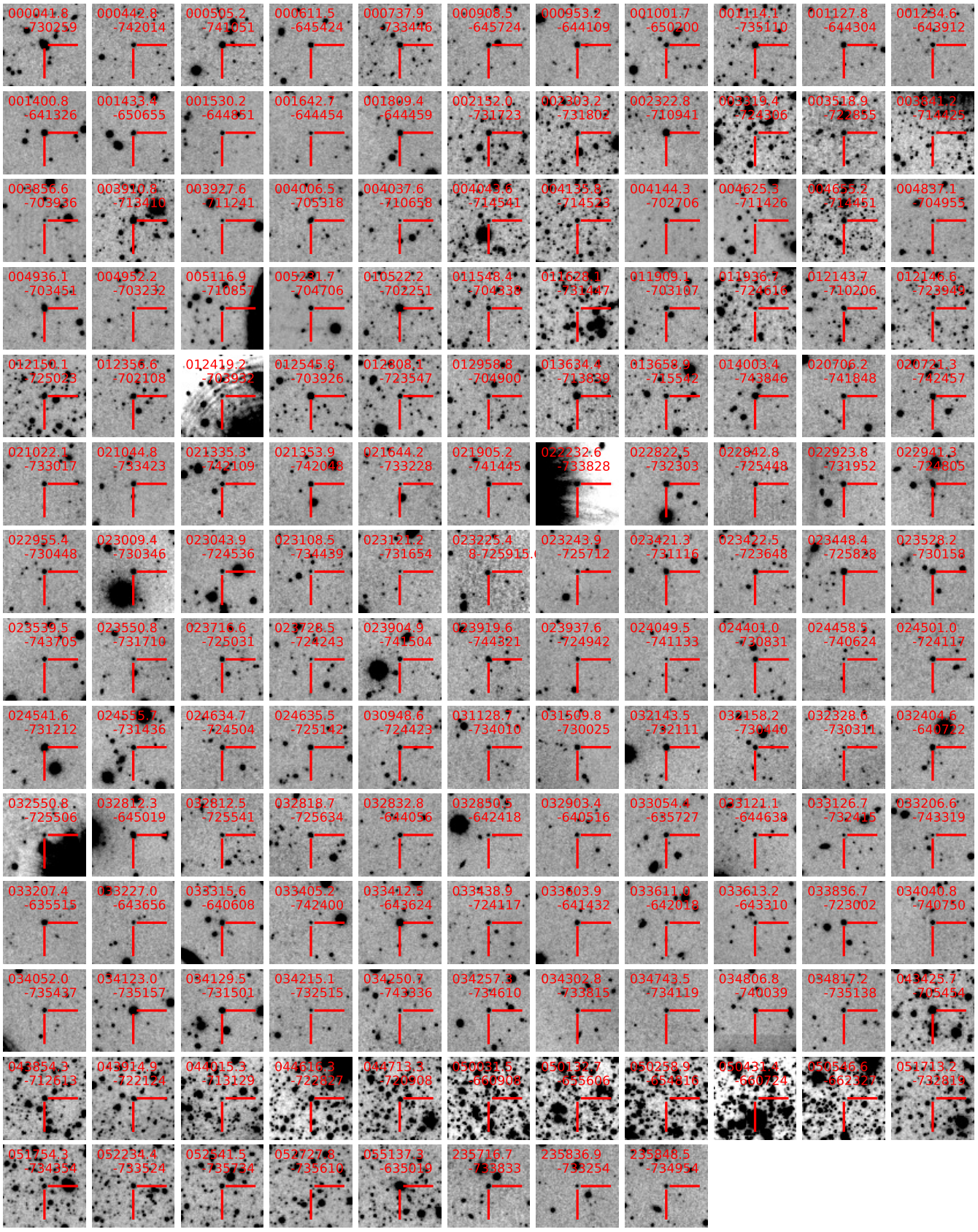

Fig. A.1. Finding charts (Y band, 1′×1′) for all 151 objects (crosses) with follow-up spectroscopy, sorted by right ascension. North is at the top, and east is to the left.

Appendix B: Complete VMC quasar candidate sample

Table B.1 lists 3609 objects that match our color and variability selection criteria. The comparison with the Quaia catalog indicates that we identify about 7% of their $G \leq 20{,}5$ mag quasars (see Sect. 4).

A SIMBAD search within 5″ from the VMC positions yielded 117 matches:

- 97 are known quasars, active galaxies, X-ray, radio, or blue-UV sources that may be consistent with galactic activity, or candidates of any of these classes;
- 16 are classified as stars. Long-period variables and young stellar objects constitute the largest consistent groups with five and three entries, respectively;
- 2 are galaxies;
- 2 are objects of an unknown nature.

Table B.1. A complete list of quasar candidates in the VMC survey.

VMC ID	α (J2000) (h:m:s)	δ (d:m:s)	G (mag)	σ_G (mag)	Y (mag)	σ_Y (mag)	J (mag)	σ_J (mag)	K_S (mag)	σ_{K_S} (mag)	Slope	$\sigma_{\rm Slope}$	N, ep.	ΔT, yrs
VMC 00:38:25.82−75:02:58.6	00:38:25.82	−75:02:58.6			19.800	0.045	19.296	0.042	17.724	0.027	−0.00011	0.00003	48	6.16
VMC 00:41:56.95−75:39:04.6	00:41:56.95	−75:39:04.6	20.004	0.008	19.336	0.032	19.216	0.039	17.866	0.029	0.00018	0.00003	48	6.16
VMC 00:33:01.86−75:44:18.1	00:33:01.86	−75:44:18.1			19.850	0.047	19.587	0.054	18.434	0.044	0.00017	0.00005	47	6.16
VMC 00:42:22.73−75:32:55.8	00:42:22.73	−75:32:55.8			19.917	0.049	19.519	0.050	18.378	0.042	−0.00015	0.00005	46	3.11
VMC 00:42:33.89−74:48:23.9	00:42:33.89	−74:48:23.9	20.369	0.010	19.458	0.035	19.337	0.043	18.100	0.034	0.00014	0.00001	87	8.08
VMC 00:33:38.37−75:44:43.8	00:33:38.37	−75:44:43.8			19.715	0.043	19.192	0.040	17.578	0.025	−0.00010	0.00003	50	6.16
VMC 00:35:07.73−75:20:34.2	00:35:07.73	−75:20:34.2			19.773	0.044	19.444	0.047	18.609	0.049	0.00015	0.00004	43	6.16
VMC 00:35:06.88−75:23:14.1	00:35:06.88	−75:23:14.1	18.960	0.006	18.216	0.015	17.941	0.017	17.079	0.019	−0.00014	0.00002	51	6.16
VMC 00:44:23.42−75:35:55.1	00:44:23.42	−75:35:55.1			19.929	0.049	19.518	0.050	18.260	0.038	0.00020	0.00004	46	3.11
VMC 00:35:38.66−75:06:45.3	00:35:38.66	−75:06:45.3	19.777	0.011	18.369	0.017	18.246	0.020	16.743	0.015	−0.00012	0.00002	51	6.16

Notes. Identifiers, coordinates, VMC survey magnitudes with their errors, number of epochs, and covered time span in years are listed. The G magnitudes and errors of *Gaia* DR3 counterparts selected within a matching radius of 0.35″ are also listed. They are available for 1249 candidates). Only part of the table is shown for guidance. The entire dataset is available at the CDS.